Relating seismic velocities, thermal cracking and permeability in Mt. Etna and Iceland basalts.

Sergio Vinciguerra[1], Concetta Trovato[1], Philip G Meredith[2], Philip M Benson[2]

[1]Osservatorio Vesuviano-Istituto Nazionale di Geofisica e Vulcanologia, Via Diocleziano 328, 80124, Naples, Italy
[2]Department of Earth Sciences, University College London, Gower Street, London, WC1E 6BT, U.K.

Abstract

We report simultaneous laboratory measurements of seismic velocities and fluid permeability on lava flow basalt from Etna (Italy) and columnar basalt from Seljadur (Iceland). Measurements were made in a servo-controlled steady-state-flow permeameter at effective pressures from 5 to 80 MPa, during both increasing and decreasing pressure cycles. Selected samples were thermally stressed at temperatures up to 900°C to induce thermal crack damage. Acoustic emission output was recorded throughout each thermal stressing experiment.

At low pressure (0 – 10 MPa), the P-wave velocity of the columnar Seljadur basalt was 5.4 km/s, while for the Etnean lava flow basalt it was only 3.0 to 3.5 km/s. On increasing the pressure to 80 MPa, the velocity of Etnean basalt increased by 45 to 60%, whereas that of Seljadur basalt increased by less than 2%. Furthermore, the velocity of Seljadur basalt thermally stressed to 900°C fell by about 2.0 km/s, whereas the decrease for Etnean basalt was negligible. A similar pattern was observed in the permeability data. Permeability of Etnean basalt fell from about $7{,}5 \times 10^{-16}$ m^2 to about $1{,}5 \times 10^{-16}$ m^2 over the pressure range 5 to 80 MPa, while that for Seljadur basalt varied little from its initial low value of 9×10^{-21} m^2. Again, thermal stressing significantly increased the permeability of Seljadur basalt, whilst having a negligible effect on the Etnean basalt. These results clearly indicate that the Etnean basalt contains a much higher level of crack damage than the Seljadur basalt, and hence can explain the low velocities (3 to 4 km/s) generally inferred from seismic tomography for the Mt. Etna volcanic edifice.

Introduction

The complex stress field acting in active volcanic areas is generated by the combined effects of regional tectonics and transient local stresses caused by magma rise into feeder dykes. Hence, the most evident precursors to volcanic activity are increases in seismicity and ground deformation, caused by magma distorting the crust as it pushes its way to the surface [1]. Improvements in volcano monitoring techniques have resulted in interpretative models of the physical changes of the edifice associated with the renewal of activity of volcanic systems. However, accurate and meaningful interpretation of the relationship between the build-up of tectonic and magmatic stresses and precursory deformation requires a-priori knowledge of the changing physical and mechanical properties of the associated rocks. The high level of mechanical and thermal stresses acting in volcanic areas, along with circulation of fluids at high temperatures, are believed to enhance mechanical damage of the host rocks to cyclic magmatic pressurisations, leading to the failure of rocks over extended periods of time at stresses far below their short-term failure stress, through mechanisms such as stress corrosion crack growth [2]. The physical state of the host rock has been recognised as crucial in determining preferential penetration of magma or steam in local fractures [3], hydrofracturing by magma injection, development of shear zones during indentation [4], and the response to the pressurization of fluids within the rock matrix [5,6]. Magmatic pressure distributions and edifice failure episodes will then depend on a high number of variables, given by the size, orientation, degree of alignment, aspect ratio and, importantly, fluid content; and from the micro to the macro scale. Thus, understanding the dynamics of volcanic systems requires the

determination of physical properties of volcanic rocks as a function of the extrinsic conditions of stress state, pressure and temperature.

Importantly, simultaneous inversion of P and S wave arrivals is a standard technique [7,8] to carry out seismic tomography in volcanic areas. P and S wave velocity increases and decreases have been interpreted as due to cooling intrusive bodies or molten rocks [e.g. 9,10]. However, despite the improvement in local seismic tomography techniques, no corresponding direct measurements are available and there is a paucity of quantitative experimental data.

Reliable laboratory measurements of physical properties, such as seismic velocity and permeability under simulate *in-situ* conditions, are therefore essential for meaningful interpretation of seismic data at the field scale, and the validation of theoretical models; a point that has been stressed by many authors [e.g. 11-15]. Vanorio et al. [16] have previously reported P-wave and S-wave velocity data for volcanic rocks, including some from Etna. However they report only dry measurements relative to exhumed old intrusive bodies.

In this study, we are concerned with investigating the physical properties of typical basalts forming the edifice of active volcanoes, built up by a pile of lava flows, and comparison with intrusive magma bodies. We therefore used material obtained from extruded lava flows from Mt. Etna volcano, Italy. Mt. Etna is a basaltic shield volcano, and is the largest continental volcano in Europe. It is continuously active, and has a basal diameter of 40 km and a height of a little over 3,000 m above sea level. It is formed from a lava flow pile, and exposures through ancient volcanic sequences show that the volume of pyroclastic material in the sequence is essentially insignificant [17]. As a basis for comparison, we have also investigated the physical properties of samples of fresh, columnar basalt, formed in an intrusive environment, from Seljadur

in the south of Iceland. For brevity, we will use the acronym EB for Etnean basalt and SB for Seljadur basalt throughout the remainder of this paper.

We report simultaneous laboratory measurements of seismic velocities and fluid permeability at confining pressures from 5 to 80 MPa; approximately equivalent to depths from 0.3 to 3.5 km. Measurements were made in a servo-controlled steady-state-flow permeameter, during both increasing and decreasing pressure cycles. In order to investigate the effect of thermal stress on the physical properties of basalt, selected samples were thermally stressed to temperatures up to 900°C to induce thermal crack damage. Acoustic emission output was recorded throughout each thermal stressing experiment.

Methodology

The material from Etna (EB) is a porphyritic alkali basalt [18] with an initial density of 2860 ± 10 kg/m^3 and a porosity of 2.1% (Figure 1a). The material from Iceland (SB) is a tholeiitic basalt with an initial density of 2900 ± 10 kg/m^3 and a porosity of around 1% (Figure 1b).

Preliminary ultrasonic wave velocity measurements were made on cylindrical samples 38 mm in diameter by 40 mm long to characterize the test materials under ambient conditions. A 900 volt pulser was used to excite a 1 MHz resonant frequency piezo-electric transmitting transducer. Waveforms captured from an identical receiver

were first pre-amplified and then recorded and displayed on a digital storage oscilloscope. Radial measurements were made in 10° increments around the circumference of each sample.

P-wave and S-wave velocity measurements were subsequently performed inside an hydrostatic pressure vessel, using silicone oil, equipped for measuring P and S-wave velocity with two 1 MHz piezo-electric resonance frequency transducer crystals, one each for compressional and shear mode. Accuracy of first arrival gives errors of 1-4%.

Two 70 MPa servo-controlled fluid pressure intensifiers (volumometers) were used to provide pore pressure independently to each end of the sample. Since the inner piston position inside the volumometer is monitored by a Linear Variable Differential Transformer (LVDT), pore volume change was measured from the water volume expelled during increasing of confining pressure (P_c) , because of closing of voids. Pore pressure (P_p) and minimum effective pressure ($P_e = P_c - P_p$) has been set at 5 MPa. P_e has been increased by steps of 5 MPa till 40 MPa and of 10 MPa till 80 MPa. A pore fluid pressure gradient between the two volumometers has been set at 0.2-0.5 MPa for measuring permeability, according to the Darcy's law (Figure 2). See Benson et al. [19]; this volume for further details.

Thermal treatment

Since volcanic areas are characterized by high temperatures at shallow depths, we also investigated how thermal stressing can induce additional crack damage into the microstructure of our rocks, and the influence this has on their physical and transport properties. Selected samples were therefore heated to temperatures of 300°,

600° and 900°C at a rate of 1°C per minute inside a tube furnace, and then allowed to cool to room temperature at the same rate. Acoustic emission (AE) output was recorded throughout each thermal stressing experiment in order to monitor the evolution of thermally-induced cracking. A schematic diagram of the experimental arrangement is given as Figure 3. A detection threshold of 35 dB was set to eliminate background laboratory noise, and the measurement transducer was located outside the furnace at the end of a stainless steel waveguide.

AE recorded during heating indicates a marked difference in behaviour between the two rocks (SB and EB) as shown in Figure 4. For SB the cumulative number of events increases continuously, with a higher event rate from about 400° to 700°C, where the bulk of the AE energy is released. A lower number of events is recorded for EB, and they are generated in episodic bursts of activity at low temperature (20° to 150°C), and around 400°C. This indicates that EB may contain a high level of pre-existing crack damage; probably due to the fast rate of cooling in lava flows. By contrast, SB is a more homogeneous material formed at a much slower rate of cooling in an intrusive environment.

Results and Discussion

Radial P-wave velocity measurements made as a function of azimuth under ambient pressure are reported in Table 1. Values for non-heat-treated EB range from 3.05 to 3.43 km/s. These values are very low for a basalt. Since the porosity is also

rather low [16], this suggests that EB contains a high density of pre-existing microcracks. However, within individual samples, the velocity anisotropy ranges from only 4 to 7%, indicating that both the matrix and the crack population are relatively isotropic. Supporting evidence comes from the measurements on the thermally stressed samples. Even after thermal stressing to 900°C, radial P-wave velocities for EB do not show any significant change (Figures 5a and 5b). This suggests that relatively few new cracks have been introduced by the thermal treatment.

Results of comparable measurements on samples of SB are in marked contrast. Azimuthal P-wave velocities for untreated SB (Table 1) range from 5.28 to 5.42 km/s, with an anisotropy of less than 3%. These velocities are more typical of a fresh, relatively unfractured basalt. Consequently, after thermal stressing to 900°C, velocities decrease significantly by more than 40% to lie in the range 3.13 to 3.18 km/s (Table 1 and Figure 6). This suggests that many new, thermally-induced cracks were generated during the thermal treatment process.

The AE generated during thermal stressing supports these observations, and suggests that EB contains many pre-existing cracks that re-open during heating and close again during cooling. By contrast, considerable crack damage is generated during heating of SB, and this reduces the P-wave velocity significantly.

Subsequently, simultaneous measurements of P-wave and S-wave velocities were made on both dry and water fully-saturated samples (hereafter named as “wet” samples) at effective pressure from 5 to 80 MPa. Measurements were made during both the pressurisation and depressurisation cycles on non-thermally-treated EB samples, and on samples previously heated to 300°, 600° and 900°C. Again, for purposes of comparison, measurements were made on samples of SB in the non-

thermally-treated state and samples heated to 900°C. Measurements of the change in porosity and permeability were also made at the same time on the wet samples.

At low confining pressure (5 MPa), P-wave velocities for dry samples of EB were in the range 2.94 to 3.21 km/s, while S-wave velocities ranged from 2.47 to 2.81 km/s. As effective pressure was increased to 80 MPa, these values increased from 4.71 to 4.96 km/s and 3.50 to 3.79 km/s, respectively (Table 2); an average increase of 55% for P-waves and 35% for S-waves. Significantly, no discernible change in either P or S wave velocity was observed between non-thermally-treated and thermally-treated samples, and no significant velocity hysteresis was detected (Figure 7). For dry samples of SB, the P-wave velocity for the non-thermally-treated sample increases from 5.43 to 5.85 km/s as effective pressure is increased from 5 to 80 MPa; an increase of 8%. The commensurate increase in the S-wave velocity is 4%; from 3.03 to 3.14 km/s (Table 3). In this case, however, dramatic decreases in both P-wave and S-wave velocities are observed in the thermally-treated material. Initial P-wave velocity is 3.19 km/s, and this increases by 47% to 4.69 km/s at 80 MPa. For S-waves the initial value is 2.05 km/s, and this increases by 30% to 2.64 km/s at 80 MPa. Again no velocity hysteresis is observed. Figure 8 shows that the initial velocities are some 70% and 30% lower in the thermally-treated SP, for P and S waves respectively. However, the increase in velocity with increasing effective stress is about an order of magnitude higher for the thermally-treated material.

Taken together, these observations provide strong evidence for a very high crack density in EB in its as-received state. Increasing the effective pressure closes many of these cracks, resulting in a significant increase in both P-wave and S-wave velocities. The absence of hysteresis suggests that during depressurisation the cracks re-open and, hence, the velocity values are recovered. Conversely, SB exhibits

considerably higher P-wave and S-wave velocities in its as-received state; by about 2.3 km/s and 1.0 km/s, respectively. It is virtually insensitive to changes in effective pressure (Figure 9a). This is indicative of an almost crack free material. However, when it is thermally stressed, many new cracks are generated, the wave velocities decrease to values very close to those for EB, and the effect of pressure becomes significant (Figure 9b).

As expected, P-wave velocities were significantly higher in wet samples of EB. More surprisingly, S-wave velocities were also higher for the wet samples. P-wave velocities ranged from 5.35 ± 0.13 km/s at 5 MPa to 5.88 ± 0.12 km/s at 80 MPa; while S-wave velocities ranged from 3.30 ± 0.04 km/s to 3.60 ± 0.04 km/s over the same pressure interval (Table 4). These velocity increases of about 10% are associated with a 25% decrease in porosity, i.e. from about 2% to about 1.5% (Figure 10). Figure 11 shows that, again, there is no discernible change in either velocity as a function of thermal stressing temperature, and no hysteresis. Similar results are seen for the wet sample of SB that had been thermally stressed to 900°C (Table 5). P-wave velocity increased from 5.16 km/s at 5 MPa to 5.80 km/s at 80 MPa; and S-wave velocity increased from 3.22 km/s to 3.62 km/s. No data is available for non-thermally-stressed SB since it was impractical to fully saturate this material over the time-scale of the experiment due to its ultra-low permeability [22].

Fluid-filled cavities enhance the propagation of seismic waves and, when combined with crack closure due to the increase in effective pressure, explains both the higher velocities observed and their lower rate of increase with effective pressure. Once again, the similarity between velocity values for both thermally and non-thermally treated EB, and thermally-treated SB is strongly supports presence of a significant level of crack damage.

Finally, Figure 12 shows how the permeability of EB decreased almost fivefold from about $7x10^{-16}$ m^2 at an effective pressure of 5 MPa to about $1x10^{-16}$ m^2 at 80 MPa. Most of the decrease (60-70%) occurs by 30 MPa, somewhat similar to the porosity decrease (Figure 10) and corresponding to the highest increase of seismic velocities. By contrast, the permeability of untreated SB has previously been found to vary little with pressure from its initial low value of $9x10^{-21}$ m^2 [22]. However, Figure 12 shows that thermal stressing has significantly increased the permeability of SB to 200 mD at 5 MPa having a negligible effect on EB.

These results clearly demonstrate that lava-flow basalt from Etna contains a much higher level of crack damage than the columnar basalt from Iceland that is formed in an intrusive environment. Our results can explain the low seismic velocities (approximately 3 to 4 km/s) inferred for basaltic volcanic edifices, which are essentially formed from piles of lava flows, and the higher values (approximately 5 to 6 km/s) observed for intrusive cooled magma bodies, such as dykes emplaced in the volcanic edifice [9,10, 20,21].

Conclusions

We reported measurements of seismic velocities and fluid permeability on lava flow basalts from Etna (Italy) and columnar basalts from Iceland at effective pressures

from 5 to 80 MPa. Selected samples were thermally stressed at temperatures up to 900°C to induce thermal crack damage.

The results demonstrate that the microstructure of erupted lava flows exhibit significantly different physical properties in comparison with columnar basalts formed in an intrusive environment. In detail the main implications are that:

- At low effective pressure, P wave velocity for the columnar Icelandic basalt was 5.4 km/s, while for the Etnean lava flow basalt it was only 3 to 3.5 km/s. On increasing the pressure to 80 MPa, velocities of Etnean basalt increased by 45 to 60%, whereas those of Icelandic basalt changed by only 4 to 5%.

- The velocity of samples of SB thermally stressed to 900°C fell by about 2.0 km/s, whereas the decrease for thermally stressed samples of EB was negligible;

-Permeability of EB fell from about $7x10^{-16}$ m^2 to about $1x10^{-16}$ m^2 over the pressure range considered, while that for SB varied little from its initial low value of $9x10^{-21}$ m^2. Again, thermal stressing significantly increased the permeability of SB ($2x10^{-16}$ m^2), whilst having a negligible effect on the EB.

- The main implication is that Etna basalts contain much higher levels of pre-existing crack damage than the Icelandic material. This results in EB having much lower seismic velocities than is generally assumed. This is consistent with *the low* seismic velocities (3 to 4 km/s) measured for basaltic volcanic edifices.

These results clearly demonstrate the importance of understanding the details of specific rock physical properties, and how they change in response to pressure and temperature, in interpreting models derived from the results of field-scale monitoring of active volcanoes.

Acknowledgements. This work has been supported by EU contract EVG1-CT-2001-00047 and by The British Council exchange, which allowed S.V. and C.T. to work in the Department of Earth Sciences, University College London, under its Anglo-Italian scientific exchange programme.

References

[1] Kilburn, C.R.J., 2003, Multiscale fracturing as a key to forecasting volcanic eruptions, Journ. Volc. Geoth. Res., 2623, 1-19.

[2] Atkinson, B.K. and Meredith, P.G., 1987, The theory of subcritical crack growth with application to minerals and rocks, In: Fracture Mechanics of Rock, Academic Press, 111-166.

[3] Chouet, B.A.,1996, Long-period volcano seismicity: its source and use in eruption forecasting. Nature 380: 309-316.

[4] Donnadieu, F. and Merle, O. 1998, Experiments on the indentation process during cryptodome intrusions: new insights into Mount St. Helens deformation. Geology. 26,1, 79-82.

[5] Voight, B. and Elsworth, D. 1997, Failure of volcano slopes. Geotechnique 47(1),1-31.

[6] Elsworth, D. and Voight, B., 2001, The mechanics of harmonic gas pressurization and failure of lava domes, 145, 187-198.

[7] Thurber, C.H., 1983, Local earthquake tomography: velocity and *Vp/Vs*-theory, In: Iyer, H.M., Hirahara, K. (Eds), Seismic Tomography: Theory and Practice. Chapman and Hall, London, pp. 613-643.

[8] Eberhart-Phillips, D., Michael, A.J., 1998, Local earthquake tomography: earthquake source regions. In: Iyer, H.M., Hirahara, K. (Eds), Seismic Tomography: Theory and Practice. Chapman and Hall, London, pp. 613-643.

[9] De Luca, G., Filippi, L., Patane', G., Scarpa R., Vinciguerra, S., 1997, Three-dimensional velocity structure and seismicity of Mt. Etna volcano, Italy, J. Volc. Geoth. Res., 79, 123-138.

[10] Patane' D., Chiarabba C., Cocina O., De Gori P., Moretti M., Boschi E., 2002, Tomographic images and 3D earthquake locations of the seismic swarm preceding the 2001 Mt. Etna eruption: Evidence for a dyke intrusion, 29, 10, 10.1029/2001GL014391.

[11] Fountain, D.M., Salisbury, M.H., Percival, J., 1990, Seismic structure of the continental crust based on rock velocity measurements from the Kapuskasing uplift. J .Geophys. Res., 95, 1167-1186.

[12] Sellami, S., Barblan, F., Mayerat, A.M., Pfiffner, O.A., Risner, K., Wagner, J.J., 1990, Compressional wave velocities of samples from NFP-20 East profile. Mem. Soc. Geol. Franc.

[13] Mueller, H.J., 1995, Modelling the lower crust by simulation of the in situ conditions; an example from the Saxonian Erzgebirge, Phys. Earth. Plan. Int., 92, 3-15.

[14] Kern, H., Gao, S., Jin, Z., Popp, T., Jin, S., 1999, Petrophysical studies on rocks from the Dabie ultrahigh-pressure (UHP) metamorphic belt Central China: implications for the composition and delamination of the lower crust. Tectonophysics, 301, 191-215.

[15] Main, I, 1996, Statistical physics, seismogenesis and seismic hazard, 1996, Review of Geophysics, 34/4, 433-462.

[16] Vanorio, T., Prasad, M., Patella, D., Nur, A., 2002, Ultrasonic velocity measurements in volcanic rocks: correlation with microtexture, Geophys. J. Int., 149, 22-36.

[17] Guest J.E., 1982, Styles of eruption and flow morphology on Mt. Etna. Mem. Soc. Geol. It., 23, 49-73.

[18] Tanguy J.C., Condomines M., Kieffer G., 1997, Evolution of Mount Etna magma: constraints on the present feeding system and eruptive mechanism. J. Volc. Geoth. Res., 75, 221-250.

[19] Benson, P.M., Meredith, P.G., Platzman, E.S., White, R.E., Pore fabric shape anisotropy in porous sandstome and its relation to elastic and permeability anisotropy under hydrostatic pressure, submitted to IJRM (this volume).

[20] Villasenor, A., Benz, H.M., Filippi, L., De Luca, G., Scarpa, R., Patanè, G., Vinciguerra, S., 1998. Three-dimensional P-wave velocity structure and of Mt. Etna, Italy. Geophysical Research Letters, 125, 11, 1975-1978.

[21] Laigle, M., Hirn, A., Sapin, M., Lepine, J.C., Diaz, J., Gallart, J., Nicolich, R., 2000. Mount Etna dense array local earthquake P and S tomography and implications for volcanic plumbing. J. Geophys. Res., 105 (B9), 21,633-21,646.

[22] Jones, C., and Meredith, P., 1998, An experimental study of elastic wave propagation anisotropy and permeability anisotropy in an illitic shale, Eurock 98, Proc. SPE/ISRM Rock Mechanics in Petroleum Engineering, Vol, 2, 307-314.

Tab. 1 – EB and SB ambient pressure measurements as a function of azimuth

	Degree	0	20	40	60	80	100	120	140	160	180	200	220	240	260	280	300	320	340
v_p [km/s]	EB_01 nott	3,24	3,20	3,20	3,15	3,20	3,38	3,38	3,27	3,22	3,22	3,27	3,15	3,20	3,20	3,35	3,35	3,35	3,30
	EB_01 tt900°	3,32	3,35	3,32	3,32	3,32	3,40	3,32	3,32	3,32	3,32	3,32	3,40	3,35	3,32	3,40	3,40	3,38	3,35
	EB_04 nott	3,20	3,08	3,15	3,05	3,15	3,05	3,08	3,20	3,17	3,20	3,17	3,10	3,12	3,12	3,10	3,22	3,22	3,22
	EB_04 tt900°	3,22	3,32	3,32	3,24	3,22	3,27	3,32	3,27	3,32	3,22	3,30	3,22	3,22	3,22	3,22	3,15	3,22	3,32
	EB_05 nott	3,43	3,32	3,32	3,32	3,32	3,32	3,35	3,40	3,38	3,40	3,40	3,32	3,38	3,22	3,32	3,40	3,43	3,38
	EB_05 tt900°	3,32	3,24	3,32	3,32	3,35	3,40	3,32	3,40	3,40	3,32	3,32	3,32	3,35	3,32	3,38	3,40	3,43	3,40
	EB_07 nott	3,15	3,27	3,23	3,17	3,11	3,10	3,12	3,05	3,20	3,22	3,30	3,27	3,17	3,20	3,10	3,15	3,15	3,22
	EB_07 tt900°	3,22	3,20	3,22	3,14	3,08	3,14	3,08	3,14	3,22	3,17	3,22	3,22	3,14	3,20	3,14	3,14	3,22	3,24
	SB_01 nott	5,31	5,36	5,36	5,42	5,42	5,39	5,31	5,31	5,42	5,31	5,31	5,36	5,42	5,42	5,42	5,31	5,28	5,31
	SB_01 tt900°	3,17	3,15	3,15	3,14	3,17	3,17	3,16	3,16	3,17	3,15	3,13	3,15	3,17	3,16	3,18	3,16	3,14	3,16

Tab. 2 – EB dry measurements vs. confining pressure

	P_c [MPa]	5	10	15	20	25	30	35	40	50	60	70	80
V_p [km/s]	**EB_01**	2.94	3.33	3.57	3.74	3.87	4.01	4.08	4.40	4.40	4.44	4.62	4.72
	EB_02	3.29	3.49	3.61	3.76	3.88	3.95	4.22	4.22	4.33	4.52	4.61	4.71
	EB_04	3.49	3.67	3.90	4.00	4.11	4.30	4.39	4.39	4.56	4.75	4.85	4.96
	EB_10	3.21	3.51	3.62	3.77	3.90	3.97	4.04	4.11	4.31	4.52	4.61	4.77
V_s [km/s]	**EB_01**	-	1.87	1.95	2.00	2.05	2.11	2.16	2.20	2.27	2.44	2.49	2.55
	EB_02	2.81	2.98	3.09	3.15	3.20	3.27	3.34	3.40	3.48	3.58	3.66	3.76
	EB_04	2.47	2.60	2.71	2.81	2.88	2.98	3.06	3.12	3.23	3.32	3.42	3.50
	EB_10	2.66	2.79	2.88	2.97	3.06	3.15	3.23	3.30	3.43	3.56	3.68	3.79

Tab. 3 – SB dry measurements vs. confining pressure

	P_c [MPa]	0	5	10	15	20	25	30	35	40	50	60	70	80
V_p [km/s]	**SB_02**	3.19	3.22	3.32	3.43	3.55	3.62	3.73	3.83	3.95	4.10	4.29	4.45	4.69
	SB_03	5.43	5.51	5.66	5.72	5.72	5.72	5.75	-	5.75	5.78	5.82	5.85	5.85
V_s [km/s]	**SB_02**	2.05	2.10	2.14	2.17	2.22	2.26	2.30	2.35	2.39	2.46	2.52	2.58	2.64
	SB_03	3.03	3.06	3.07	3.08	3.08	3.08	3.09	-	3.09	3.10	3.12	3.13	3.14

Tab. 4 – EB wet measurements vs. effective pressure

	P_{eff} [MPa]	5	10	15	20	25	30	35	40	50	60	70	80
V_p [km/s]	**EB_01**	5.22	5.25	5.31	5.37	5.40	5.46	5.49	5.52	5.56	5.64	5.72	5.76
	EB_02	5.32	5.32	5.40	5.44	5.52	5.52	5.60	5.60	5.68	5.76	5.76	5.84
	EB_03	5.40	5.48	5.52	5.60	5.64	5.68	5.72	5.72	5.80	5.84	5.88	5.92
	EB_06	5.31	5.40	5.44	5.52	5.60	5.60	5.64	5.68	5.80	5.84	5.88	5.92
	EB_07	5.25	5.31	5.34	5.40	5.48	5.48	5.56	5.60	5.64	5.68	5.76	5.80
	EB_08	5.48	5.52	5.60	5.64	5.68	5.68	5.72	5.76	5.84	5.88	5.96	5.96
	EB_09	5.48	5.56	5.60	5.60	5.68	5.68	5.76	5.76	5.84	5.88	5.96	6.00
V_s [km/s]	**EB_01**	3.28	3.34	3.38	3.40	3.44	3.46	3.48	3.52	3.54	3.58	3.62	3.64
	EB_02	3.26	3.28	3.34	3.36	3.38	3.40	3.44	3.48	3.50	3.52	3.54	3.56
	EB_03	3.34	3.38	3.44	3.46	3.46	3.48	3.48	3.48	3.50	3.54	3.56	3.58
	EB_06	3.28	3.32	3.36	3.38	3.40	3.42	3.44	3.46	3.52	3.54	3.58	3.60
	EB_07	3.30	3.34	3.36	3.40	3.42	3.44	3.46	3.48	3.50	3.54	3.56	3.60
	EB_08	3.30	3.32	3.36	3.38	3.40	3.42	3.42	3.44	3.48	3.50	3.54	3.56
	EB_09	3.32	3.36	3.38	3.40	3.42	3.44	3.48	3.48	3.52	3.56	3.58	3.60

Tab. 5 – SB wet measurements vs. effective pressure

	P_{eff} [MPa]	5	10	15	20	25	30	35	40	50	60	70	80
SB_01	V_p [km/s]	5.16	5.22	5.28	5.36	5.40	5.44	5.48	5.56	5.64	5.72	5.76	5.80
	V_s [km/s]	3.22	3.26	3.30	3.36	3.38	3.42	3.44	3.46	3.52	3.54	3.60	3.62

Figure captions

Figure 1 - Optical images (SEM) of EB (a) and SB (b), after a pressurisation-depressurisation cycle.

Figure 2 - Schematic sketch of the servo controlled permeameter equipped for Vp, Vs and permeability measurements.

Figure 3 - Sketch of the experimental apparatus for thermal treatment.

Figure 4 - Amplitude vs. temperature and cumulative number of events vs. time for EB (a,b) and SB (c,d).

Figure 5 - Radial P-wave velocity for (a) untreated and (b) 900°C thermally treated EB.

Figure 6 - Radial P-wave velocity for (a) untreated and (b) 900°C thermally treated SB.

Figure 7 - P and S wave velocities vs. confining pressure for EB dry samples.

Figure 8 - P and S wave velocities vs. confining pressure for SB dry samples.

Figure 9 - Normalised P-wave velocity values for (a) untreated EB and SB samples and (b) 900° C thermally treated samples.

Figure 10 - Porosity vs. effective pressure for EB samples

Figure 11 - Averaged P and S wave velocities vs. effective pressure for EB wet samples.

Figure 12 - Permeability vs. effective pressure for EB and SB thermally treated samples.

Fig. 1

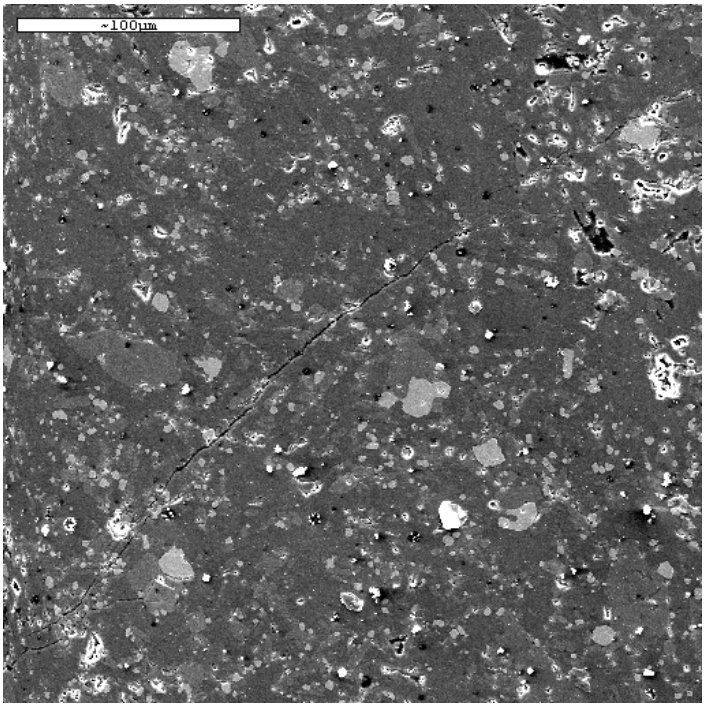

a

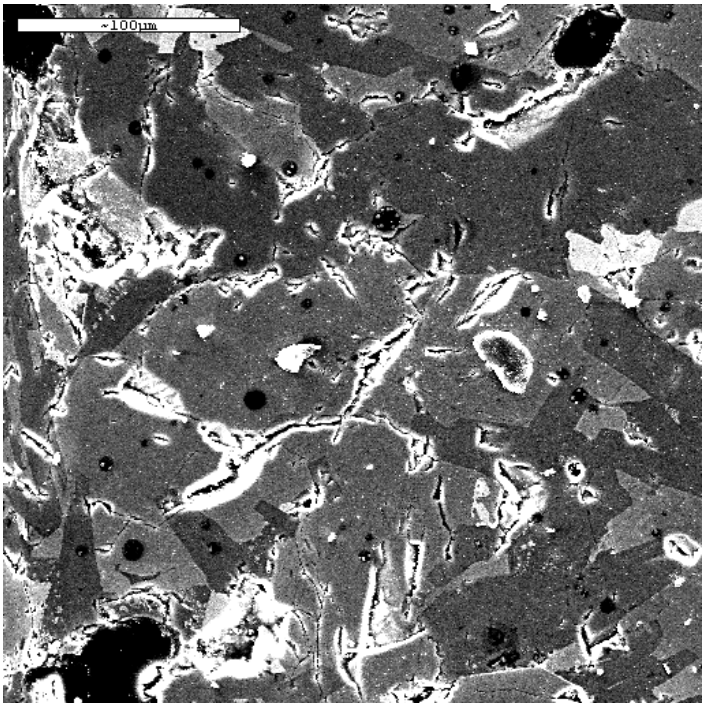

b

Fig. 2

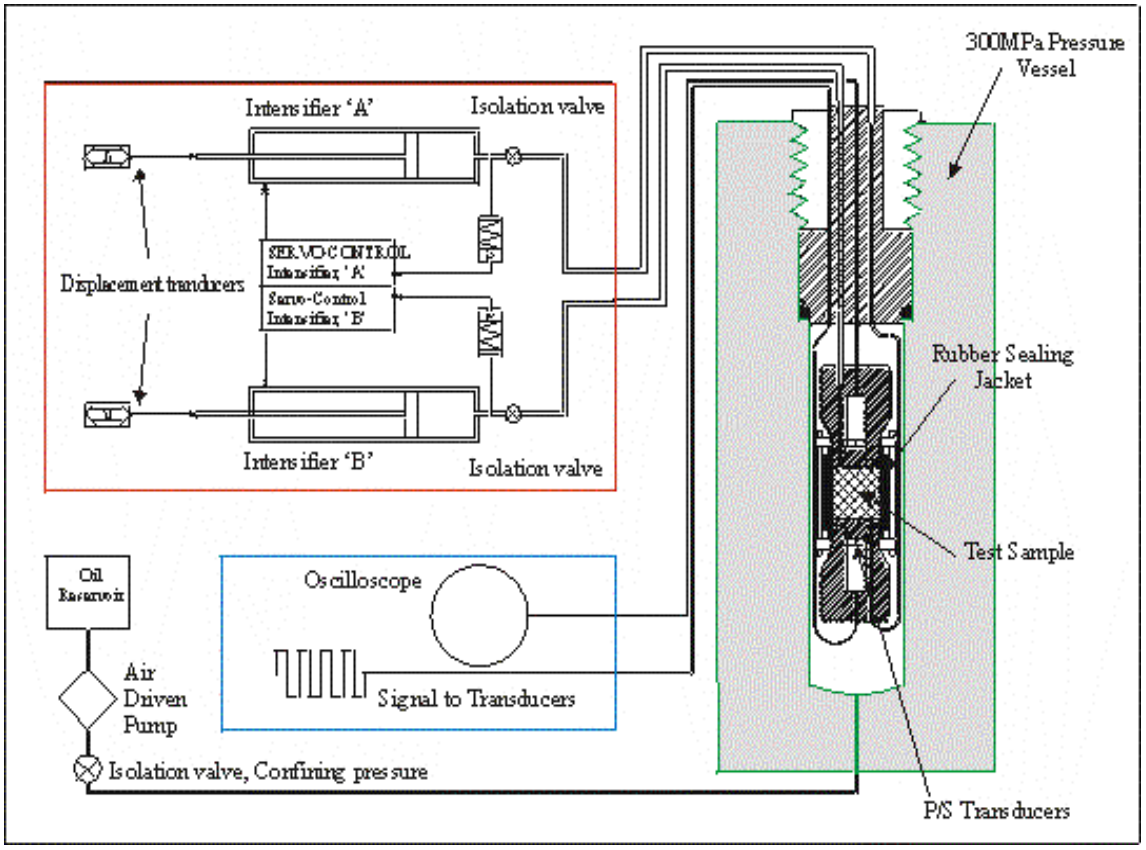
300MPa Pressure Vessel
Intensifier 'A'
Isolation valve
Displacement transducers
SERVO-CONTROL
Intensifier 'A'
Servo-Control
Intensifier 'B'
Intensifier 'B'
Isolation valve
Rubber Sealing Jacket
Test Sample
Oil Reservoir
Oscilloscope
Air Driven Pump
Signal to Transducers
Isolation valve, Confining pressure
P/S Transducers

Fig. 3

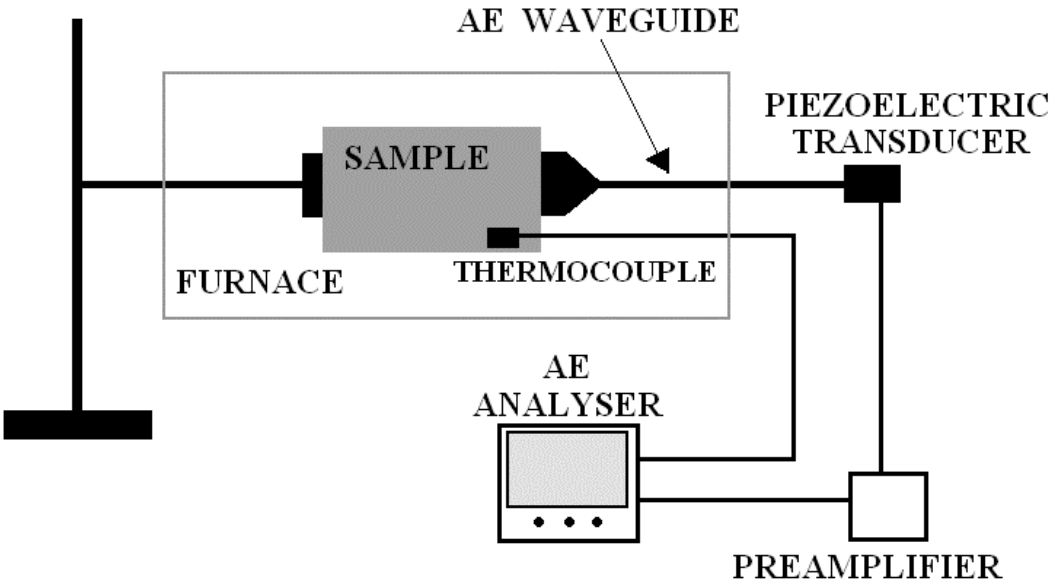
AE WAVEGUIDE
PIEZOELECTRIC TRANSDUCER
SAMPLE
FURNACE
THERMOCOUPLE
AE ANALYSER
PREAMPLIFIER

Fig. 4a,b,c,d

a

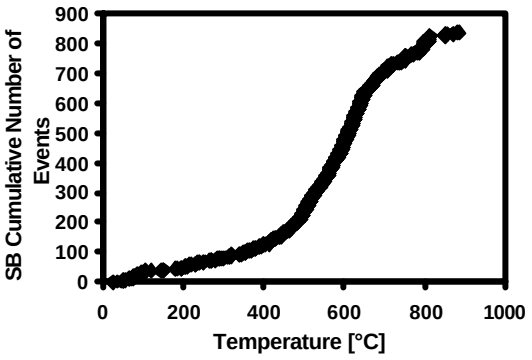

b

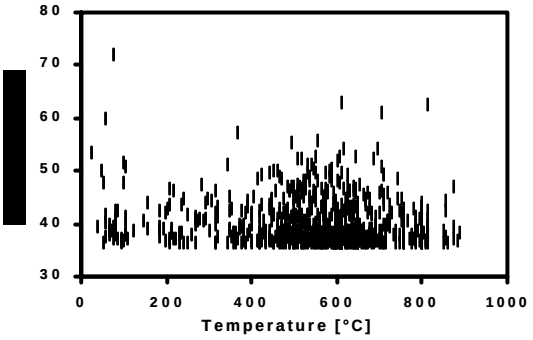

c

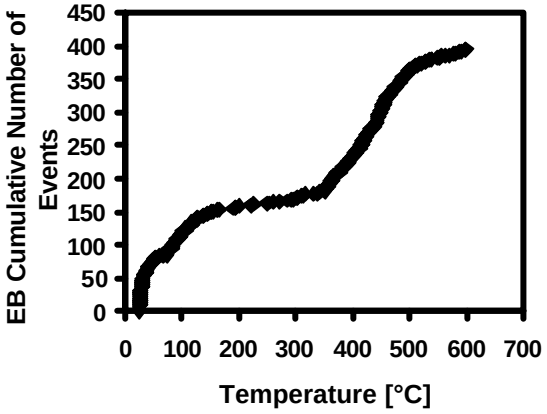

d

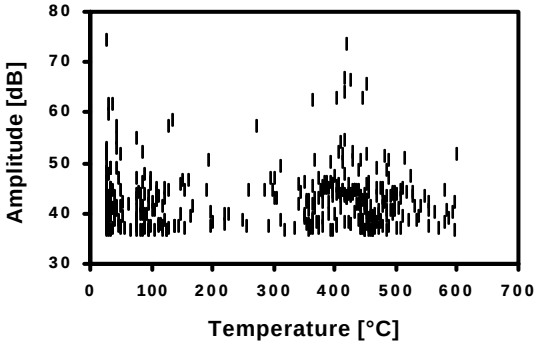

Fig. 5

a

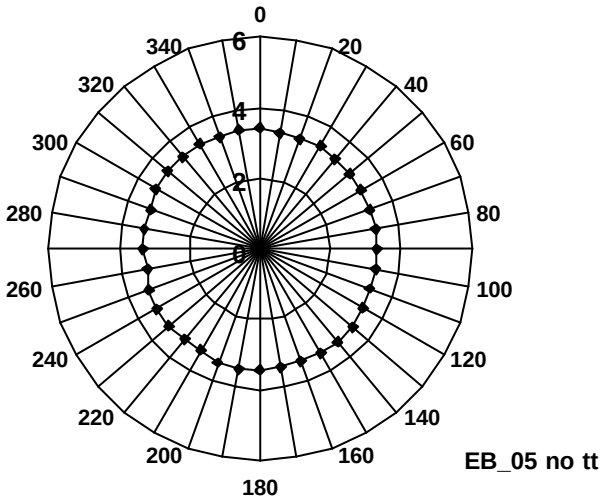
0
20
40
60
80
100
120
140
160
180
200
220
240
260
280
300
320
340
6
4
2
0
EB_05 no tt

b

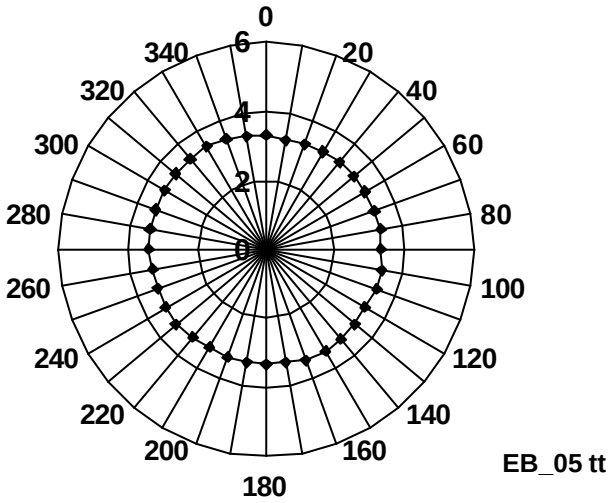
0
20
40
60
80
100
120
140
160
180
200
220
240
260
280
300
320
340
6
4
2
0
EB_05 tt

Fig. 6

a

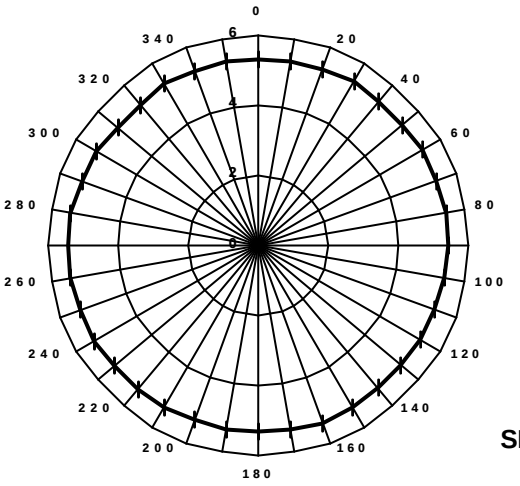

SB_01 no tt

b

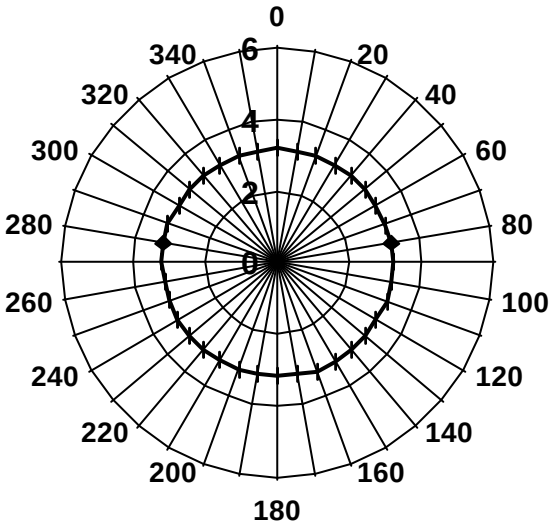

SB_01 tt

Fig. 7

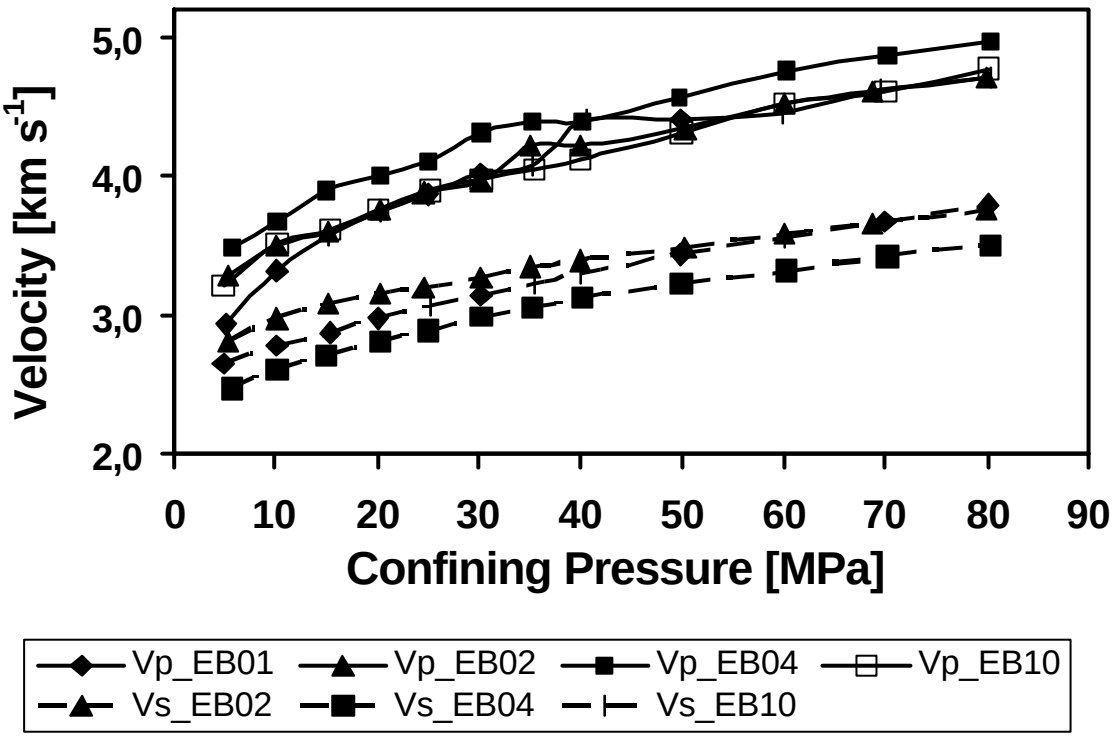
Velocity [km s-1]
5,0
4,0
3,0
2,0
0
10
20
30
40
50
60
70
80
90
Confining Pressure [MPa]
Vp_EB01
Vp_EB02
Vp_EB04
Vp_EB10
Vs_EB02
Vs_EB04
Vs_EB10

Fig. 8

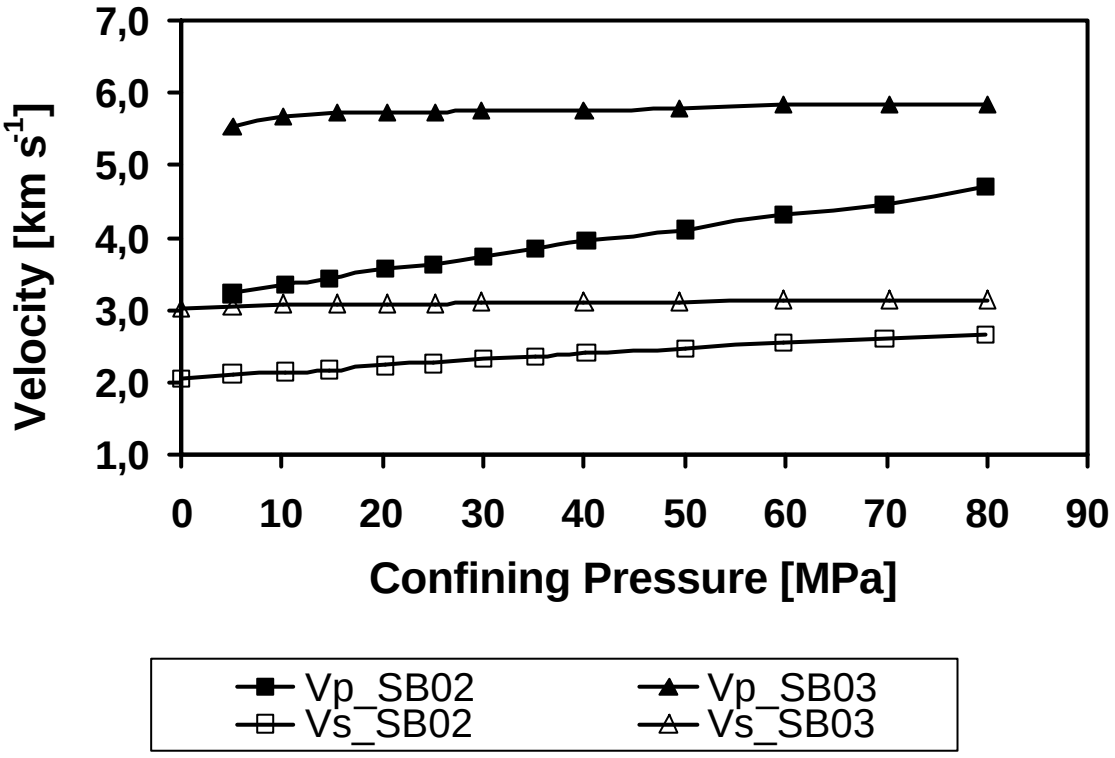
7,0
6,0
5,0
4,0
3,0
2,0
1,0
Velocity [km s-1]
0
10
20
30
40
50
60
70
80
90
Confining Pressure [MPa]
Vp_SB02
Vp_SB03
Vs_SB02
Vs_SB03

Fig. 9

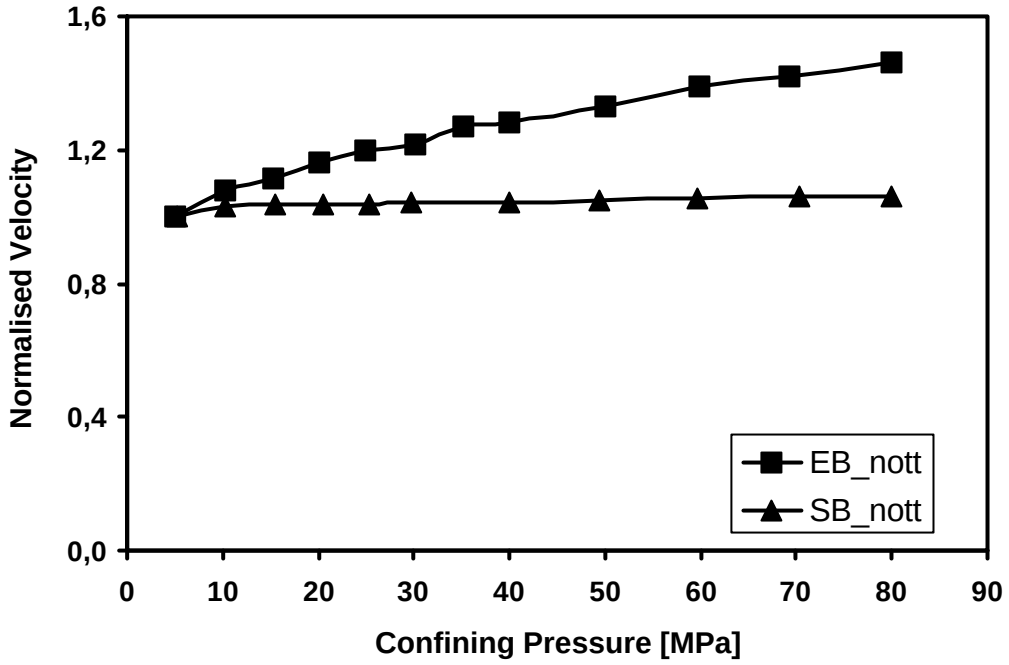
1,6
1,2
0,8
0,4
0,0
Normalised Velocity
0
10
20
30
40
50
60
70
80
90
Confining Pressure [MPa]
EB_nott
SB_nott

a

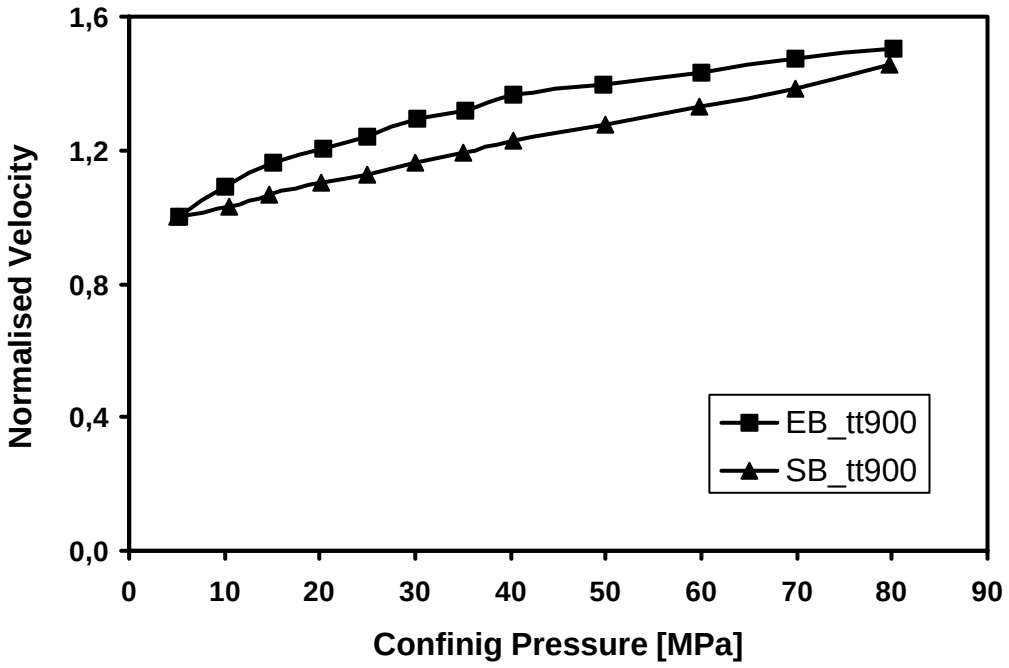
1,6
1,2
0,8
0,4
0,0
Normalised Velocity
0
10
20
30
40
50
60
70
80
90
Confinig Pressure [MPa]
EB_tt900
SB_tt900

b

Fig. 10

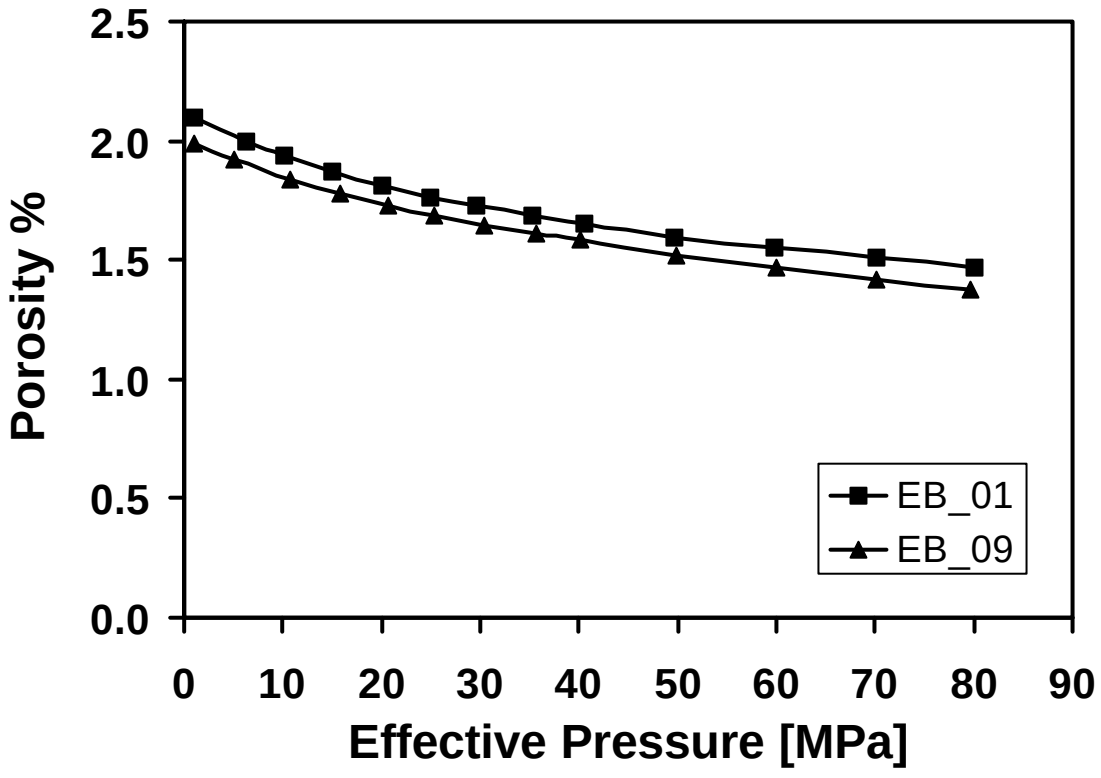
Porosity %
2.5
2.0
1.5
1.0
0.5
0.0
0
10
20
30
40
50
60
70
80
90
Effective Pressure [MPa]
EB_01
EB_09

Fig. 11

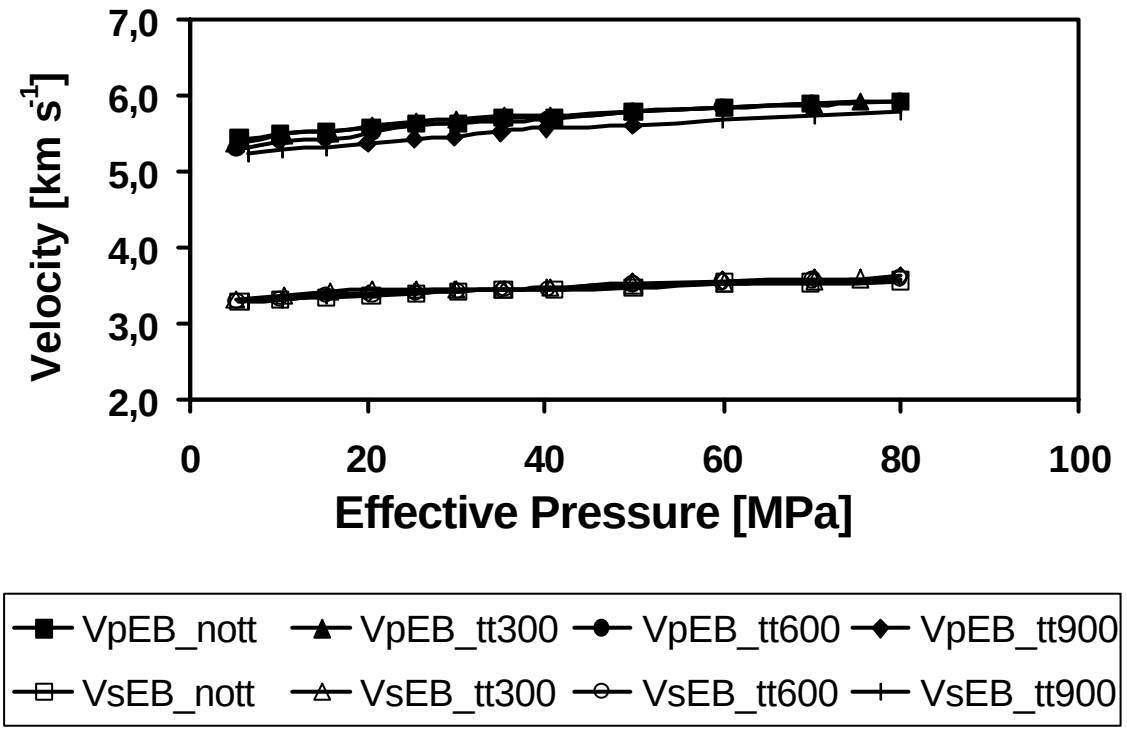
7,0
6,0
5,0
4,0
3,0
2,0
Velocity [km s-1]
0
20
40
60
80
100
Effective Pressure [MPa]
VpEB_nott
VpEB_tt300
VpEB_tt600
VpEB_tt900
VsEB_nott
VsEB_tt300
VsEB_tt600
VsEB_tt900

Fig. 12

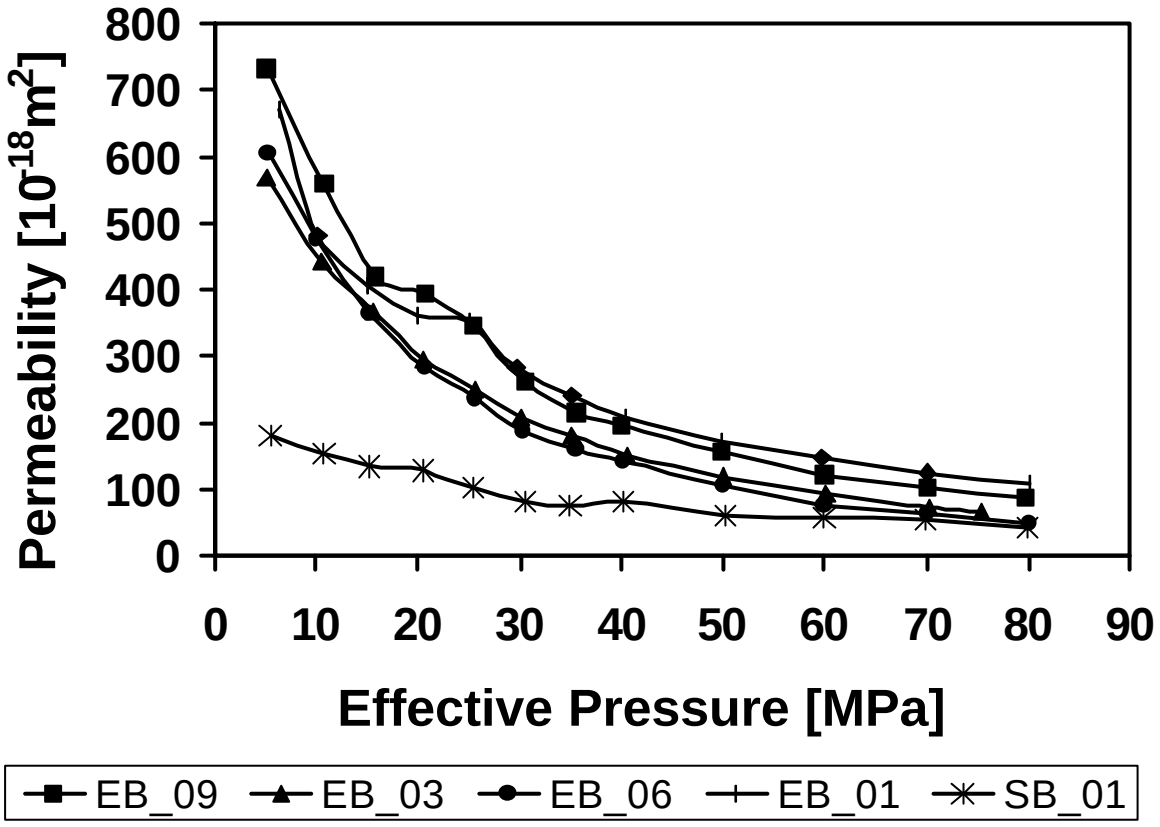
Permeability [10^-18 m^2]
800
700
600
500
400
300
200
100
0
0
10
20
30
40
50
60
70
80
90
Effective Pressure [MPa]
EB_09
EB_03
EB_06
EB_01
SB_01